Callisto and Europa Gravity Measurements from JUICE 3GM Experiment Simulation

Paolo Cappuccio [iD], Mauro Di Benedetto, Daniele Durante [iD], and Luciano Iess [iD]
Department of Mechanical and Aerospace Engineering, Sapienza University of Rome, Via Eudossiana 18, Rome, Italy; paolo.cappuccio@uniroma1.it

Abstract

The JUpiter Icy Moons Explorer is an ESA mission set for launch in 2023 April and arrival in the Jovian system in 2031 July to investigate Jupiter and its icy satellites with a suite of 10 instruments. The mission will execute several flybys of the icy moons Europa, Callisto, and Ganymede before ending the mission with a 9-month orbit around Ganymede. The 3GM experiment on board the spacecraft will exploit accurate range and Doppler (range-rate) measurements to determine the moons' orbit, gravity field, and tidal deformation. The focus of this paper is on the retrieval of Europa's and Callisto's gravity field, without delving into the modeling of their interior structures. By means of a covariance analysis of the data acquired during flybys, we assess the expected results from the 3GM gravity experiment. We find that the two Europa flybys will provide a determination of the J_2 and C_{22} quadrupole gravity field coefficients with an accuracy of 3.8×10^{-6} and 5.1×10^{-7}, respectively. The 21 Callisto flybys will provide a determination of the global gravity field to approximately degree and order 7, the moon ephemerides, and the time-variable component of the gravitational tide raised by Jupiter on the moon. The k_2 Love number, describing the Callisto tidal response at its orbital period, can be determined with an uncertainty $\sigma_{k2} \sim 0.06$, allowing us to distinguish with good confidence between a moon with or without an internal ocean. The constraints derived by 3GM gravity measurements can then be used to develop interior models of the moon.

Unified Astronomy Thesaurus concepts: Jovian satellites (872); Galilean satellites (627); Orbit determination (1175); Tides (1702); Gravitational fields (667)

1. Introduction

Jupiter Icy moons Explorer (JUICE) is the first ESA mission devoted to the exploration of Jupiter and its icy moons. The nominal launch date is in 2023 April, with the spacecraft starting its science operations in 2031 July, after the gravitational capture by Jupiter. Following an initial Ganymede flyby just a few hours before the orbit insertion maneuver, JUICE will start its tour in the Jovian system, lasting approximately 3 yr and 3 months.

Ganymede is the primary scientific objective of the entire mission. It will be thoroughly studied during a 9-month orbital phase at the end of the Jovian tour. Before entering in orbit around Ganymede, JUICE will perform interdisciplinary observations of Jupiter and of the Galilean moons Europa and Callisto, with its 10 scientific instruments. Shortly after the capture maneuver, JUICE will be put in resonant orbits with Ganymede, in the so-called energy reduction phase (ESA SPICE Service 2020), to further reduce the orbital energy and then start the Europa science phase. JUICE will perform only two flybys of Europa during the entire mission, being limited by the harsh radiation environment in proximity of the moon's orbit. Afterward, it will be put in a 1:1 resonant orbit with Callisto, using repetitive gravity assists to raise the orbit inclination and perform observations of the Jupiter atmosphere at high latitudes in the northern hemisphere. The comparative study of Europa, Ganymede, and Callisto aims at answering two of the main themes of the ESA Cosmic Vision 2015–2025 program: "What are the conditions for the planet formation and emergence of life?" and "How does the Solar System work?" (Grasset et al. 2013).

The radio science experiment on board the JUICE mission, Gravity and Geophysics of Jupiter and the Galilean Moons (3GM), aims at improving the current knowledge of the interior structure of the three moons by measuring their gravity fields and, for Callisto and Ganymede, their tidal response to the time-varying gravitational pull of Jupiter, induced by orbital eccentricity (0.0074 and 0.0011, respectively). On a global scale, the periodic variation of the moons' degree-2 gravity coefficients is described by the Love number k_2, whose accurate estimation is crucial to unambiguously confirm the presence of subsurface oceans (see, e.g., the Titan case; Iess et al. 2014). The estimation of Callisto's tidal response is one of the primary objectives of the 3GM gravity experiment. Europa's tidal response is not measurable by 3GM owing to the limited number of flybys. However, the NASA Europa Clipper mission will be able to measure the tidal Love number k_2 (Verma & Margot 2018), likely confirming the magnetic evidence for a subsurface ocean (Kivelson et al. 2000) detected by the NASA Galileo mission. The measurement of Callisto's k_2 is crucial because the magnetic induction measured by Galileo is prone to some ambiguity, making the existence of a subsurface ocean uncertain (Zimmer et al. 2000; Spohn & Schubert 2003).

3GM observations will allow measurements of Europa's and Callisto's quadrupole gravity coefficients, therefore testing the deviation of the moons from hydrosticity, i.e., if the inward acceleration due to gravity is balanced by the gradient in fluid pressure (Hemingway et al. 2018). We stress the fact that, differently from Galileo analysis (Anderson et al. 1998, 2001), 3GM will test the hydrostatic equilibrium hypothesis rather than assuming it. Recent reanalysis of Galileo data showed that the hydrostatic equilibrium hypothesis for Europa cannot be tested with the Galileo data set (Gomez Casajus et al. 2021). A negligible or small departure from hydrostatic equilibrium leads to a potential improvement of the polar moment of inertia

and a more robust measurement of the degree of differentiation, inferred from the J_2 and C_{22} by using the Radau–Darwin equation (Darwin 1899; Murray & Dermott 2000). On the other hand, if a substantial departure from the hydrostatic equilibrium will be detected, 3GM could use topographic data and higher-order harmonics of the gravity field to disentangle the hydrostatic and nonhydrostatic components of the quadrupole coefficients of the gravity field, following the approach of Iess et al. (2014, 2010). In this case, we could also detect the depth at which the surface gravity anomaly is compensated, inferring information on the ice shell. Since this approach relies on different instruments, it will be investigated in next phases of the mission planning when the operation scenarios will be fixed and thus the accuracy of the topographic and radio science data product will be solid.

In this work, we present the results of covariance analysis of both the Callisto and Europa gravity experiments, while results of numerical simulations of the 3GM Ganymede gravity experiment are reported in other works (Cappuccio et al. 2020b; de Marchi et al. 2021). As we will show and discuss here, the estimation accuracy of Callisto's gravity field and tidal response to Jupiter is strongly dependent on many orbital parameters and mission operational constraints, such as the flybys' mean anomaly distribution, timing of closest approaches, and reaction wheel off-loading occurrences. We have considered the current ESA baseline trajectory (corresponding to notional mission kernel 150l0a) and the backup option with launch in 2023 August (corresponding to mission kernel 230la, both reported in CReMA 5.0; see ESA SPICE Service 2020). The backup tour characteristics offer the possibility to test the performance of our experiment with a different mission scenario.

The paper is structured as follows: Section 2 reports the current knowledge of Callisto's and Europa's interior structure; Section 3 describes in detail the 3GM gravity experiment, while Section 4 provides a description of the setup used in our numerical simulations. Results and possible geophysical implications are discussed in Section 5. Finally, Section 6 summarizes our conclusions.

2. Models of Europa and Callisto's Interior Structure

Early observations of the Galilean moons carried out by the Pioneer and Voyager probes paved the way for the Galileo mission, which showed evidence of tectonic, volcanic, and cryovolcanic activities (except Callisto) and allowed a significant revision of preliminary models of the internal structure of the Galilean moons (Fimmel et al. 1980; Lupo 1982; Mueller & McKinnon 1988). The four Galilean satellites show an increase in geologic activity with decreasing distance from Jupiter and can be broadly divided into two subclasses: Io and Europa are rocky moons, while Ganymede and Callisto are thought to have an almost equivalent mix of rock and ice. Images from Galileo showed dramatic differences of the surfaces of the Galilean satellites. Europa's surface is sparsely cratered and younger than that of Ganymede and Callisto (Carr et al. 1998). Global ridged plains, markers of recent geologic activity, and chemical traces on the surface may suggest the presence of a global liquid ocean below the icy crust (McCord et al. 1999, 2001). On the very opposite, Callisto appears as geologically dead, showing a densely cratered terrain remnant of a heavy bombardment phase that ended about 4 Gyr ago, making the presence of a subsurface

ocean less likely. It has the lowest albedo among the four moons, suggesting a significant presence of still-unknown non-icy components on the surface.

In the pre-Galileo era, some authors already suggested the likely presence of salty water oceans beneath the surface of the two moons (Parmentier et al. 1982; Lee Allison & Clifford 1987; Schenk et al. 2001). Afterward, measurements carried out by the magnetometer on board Galileo strongly supported the existence of a subsurface ocean below Europa's icy shell (Kivelson et al. 2000). Surface morphology features revealed by Galileo's imaging system have corroborated the picture of an icy surface floating on a watery subsurface ocean (Carr et al. 1998; Pappalardo et al. 1999). Gravity measurements, assuming that Europa is in hydrostatic equilibrium, have indicated that the moon is a highly differentiated body (Anderson et al. 1997), with models preferring a Fe or a Fe–S core whose size depends on the density of the mantle and a thickness of the outer water-ice shell in the range 80–170 km (Anderson et al. 1998). Other works prefer Europa interior models with thinner icy shells in the range 15–45 km but do not exclude models with larger icy shells (Hussmann et al. 2002; Kuskov & Kronrod 2005; Vilella et al. 2020). The first attempt to also account for geochemical constraints (the composition of meteorites, in particular L- and LL-type chondrites) provided an estimate of the outer shell thickness in good agreement with previous estimates derived only from geophysical parameters (Kuskov et al. 2001). Other models have then confirmed that the thickness of Europa's icy shell is several tens of kilometers (Hussmann et al. 2002), while a further work on its interior structure, assuming either L/LL-chondritic or CM-chondritic bulk model composition, raised the likely thickness of the outer water-ice shell to the 105–160 km range and the Fe–S core radius to 505–670 km, considering mantle models either with or without a crust (Kuskov & Kronrod 2005).

Callisto has the lowest mean density (834.4 ± 3.4 kg m^{-3}) and the highest polar moment of inertia (0.3549 ± 0.0042) factor, MoIF $= C/MR^2$, among the four Galilean satellites (Anderson et al. 2001; Kuskov & Kronrod 2005; MOIF was calculated from Radau–Darwin equations, under the hypothesis of hydrostatic equilibrium). The high value of Callisto's MoIF indicates that the moon cannot be entirely differentiated. These geophysical measurements are compatible with both a two-layer model with an ice-rock-metal core and a thick ice shell (up to 350 km) and a three-layer model with an inner rock-metal core (Anderson et al. 2001). Both models show that a region with mixed ice and rock-metal is required. As for Europa, the Galileo magnetometer measured an induced field on Callisto that suggests the presence of a subsurface water ocean (Zimmer et al. 2000), but this magnetic evidence is not conclusive if water and ice are poor in salt content (Spohn & Schubert 2003). An ocean is almost certain if a 5% bulk concentration of ammonia is present in the ice (Spohn & Schubert 2003). Models of the interior structure of Callisto, taking into account the phase diagram of the H$_2$O in the region ice-I–ice-III–ice-V–liquid, show that the possible thickness of the subsurface ocean decreases linearly with the thickness of the icy crust and that the maximum ice-water thickness is 315 km (Kuskov & Kronrod 2005). The most likely thickness for the ice-I crust is 135–150 km, while the thickness of the liquid layer is 120–180 km. The value of the latter is strongly dependent on the heat flow and the thickness of the ice-I shell, while being barely dependent on the density of the rock-iron

core material. The radius of the iron-rock core depends on the core density, with 3150 kg m$^{-3} \leqslant \rho_{\mathrm{Fe-Si}} \leqslant 3620$ kg m^{-3}, and the thickness of the intermediate rock-iron mantle shall be >1100 km.

3. 3GM Experiment

The 3GM experiment has scientific objectives pertaining to (a) geodesy and geophysics of the Galilean satellites and (b) atmospheric science. These will be addressed with two different and separated units hosted on board the spacecraft, a Ka-band Transponder (KaT) and an Ultra Stable Oscillator. The latter will be used to generate a stable reference signal on board the spacecraft to carry out occultation experiments in one-way downlink mode at both X and Ka bands. The KaT will be used for gravity measurement experiments by providing very accurate two-way coherent range and Doppler (range-rate) observables at Ka band (uplink: 34 GHz; downlink: 32.5 GHz). Data from a High Accuracy Accelerometer (HAA) are also available, mostly to remove the effect of the propellant sloshing on the tracking radio measurements.

The main purpose of the Callisto gravity experiment is to unambiguously detect whether a global liquid ocean is present or not beneath the icy crust, refine models of the interior structure, assess the extent of internal differentiation and determine whether the moon is in hydrostatic equilibrium, and remove the ambiguity in the interpretation of Galileo data. For Europa, the goal is to determine independently J_2 and C_{22} gravity coefficients to refine measurements of the moment of inertia and the extent of the moon hydrosticity. 3GM has set a requirement also on the measurement of the zonal spherical harmonic of degree 3, J_3, to constrain the nonhydrostatic component of the quadrupole coefficient of the gravity field and infer the compensation depth (Iess et al. 2010).

To meet these scientific goals, the mission adopted the following L1-level requirements (as per ESA terminology), which require measuring:

1. Callisto tidal Love number k_2 with an absolute uncertainty of at least 0.06;
2. Callisto degree-3 gravity field (with an accuracy for J_3 better than 4×10^{-8});
3. Europa unconstrained J_2 and C_{22} gravity coefficients at 1%–2% relative uncertainties.

The capability of meeting such requirements, and possibly to go beyond them, is determined by 3GM data accuracy, tour design, and operational constraints imposed by the spacecraft. In addition to this, 3GM could exploit superior solar conjunctions to perform a fundamentals physics test during the cruise phase (di Stefano et al. 2019, 2022).

3.1. Measurement Technique

The mass and mass distribution of celestial bodies can be measured indirectly through the dynamical effect on test masses. The gravity field of the Galilean satellites will be therefore inferred through the accurate orbit determination of the JUICE spacecraft, by adjusting gravity coefficients (together with other dynamical model and observation parameters) to minimize differences between predicted and observed observables, forming the vector of residuals. The gravitational potential of a celestial body can be modeled through a spherical harmonic expansion with normalized

coefficient of degree l and order m ($\overline{C}_{lm}$, $\overline{S}_{lm}$):

$$
U(r, \lambda, \phi) = \frac{GM}{r} \left[1 + \sum_{l=2}^{\infty} \sum_{m=0}^{n} \left(\frac{R_E}{r} \right)^n \overline{P}_{lm}(\sin \phi) \right.
$$
$$
\left. \cdot (\overline{C}_{lm} \cos m\lambda + \overline{S}_{lm} \sin m\lambda) \right], \tag{1}
$$

where G is the gravitational constant, M is the planet or satellite mass, $\overline{P}_{nm}$ are the fully normalized associated Legendre polynomials, R_e is the reference radius of the body, and ϕ, λ, and r are, respectively, latitude, longitude, and radial distance. Because of the eccentricity of Europa and Callisto orbits, respectively $e_E = 0.0094$ and $e_C = 0.0074$ (Lainey et al. 2004), the Jupiter-induced gravitational tide is not constant along the orbit, and the moons' gravity field is time-variable. The periodic variations of the moons' quadrupole field in response to Jupiter tidal potential U_2^J are proportional to the Love number k_2, i.e., the gravity field of the moons depends on the mean anomaly of their orbit (from Equation (5) of van Hoolst et al. 2013):

$$
\Delta U_2 = k_2 \frac{1}{2} \frac{GM}{r} \left(\frac{a_E}{r} \right)^2 e \left\{ 3 \left[P_{20}(\sin \phi) - \frac{1}{2} P_{22}(\sin \phi) \cos 2\lambda \right] \right.
$$
$$
\left. \times \cos M - 2 P_{22}(\sin \phi) \sin 2\lambda \sin M \right\}, \tag{2}
$$

where e is the orbit eccentricity and M is the mean anomaly.

The mathematical formulation we used for the observational model of radiometric data (i.e., Doppler and Range observables) is described in Moyer (2003). The gravity coefficients are estimated through iterative weighted least-squares differential corrections with a priori information, given at k-step by Schutz et al. (2004):

$$
\delta \hat{x}_k = (H_k^T W_k H_k + \overline{P}_k^{-1})^{-1} (H_k^T W_k \delta \hat{y}_k + \overline{P}_k^{-1} \delta \overline{x}_k), \tag{3}
$$

where x is the unknown n-dimensional vector of the parameters to be estimated (also called solved-for parameters) and $\delta \hat{x}$ is the vector of differential corrections. H is the $p \times n$ design matrix (p is the number of observables) containing the partial derivatives of the observables with respect to the solved-for parameters. $\delta \overline{x}$ and $\overline{P}_k$ represent, respectively, the a priori estimate deviation and covariance of x. δy is the vector of residuals, i.e., the vector of differences between observed and computed observables, and W is the corresponding weighting matrix. The $n \times n$ matrix $P_k = (H_k^T W_k H_k + \overline{P}_k^{-1})^{-1}$ represents the covariance matrix of solved-for parameters, which coincides with the minimum variance estimate.

The gravity fields of Callisto and Europa are estimated by using data acquired during flybys occurring at distant epochs. In general, inaccuracies of the dynamical model, numerical rounding errors of the orbit propagators (due to finite machine number representation), and orbit maneuvers (affecting the dynamical coherence of the spacecraft trajectory) make it practically impossible to fit very long batches of radiometric data. The problem is overcome by using a multiarc approach (Milani & Gronchi 2009), in which the JUICE trajectory is split into shorter arcs and the set of dynamical parameters is divided into two categories: global and local ones. Global parameters are the ones common to all arcs (e.g., gravity coefficients), while local ones are those relevant to individual flybys (e.g., spacecraft initial state).

3.2. 3GM Data Quality

Spacecraft Doppler tracking is the most reliable technique to retrieve the orbit of a deep-space probe orbiting a distant body. The frequency shift of a radio link provides information about the spacecraft–Earth relative velocity along the line of sight, and range-rate is the primary observable to position JUICE with respect to the Galilean moons. Range data are related to the absolute distance from Earth and are sensitive to the moon/spacecraft positioning within the Jupiter system, as well as the Jupiter system's barycenter in the solar system. In the past, range data have been prone to large ground station bias errors that can lead to possible inconsistencies with Doppler data unless appropriate range biases are applied. The novel pseudo-noise (PN) code at 24.35 Mcps mitigates this problem, and the effect of range biases is significantly reduced, making range data significantly more valuable (Cappuccio et al. 2020c). Systematic errors in range-rate observations are almost negligible in the band of interest of 3GM gravity observations (10^{-4} to 10^{-1} Hz; Asmar et al. 2005).

The core of the 3GM gravity experiment is a state-of-the-art KaT manufactured by Thales Alenia Space—Italy (TAS-I), a nearly recurrent unit from the Mercury Orbiter Radio science Experiment (MORE) of the ESA/BepiColombo mission to Mercury (Genova et al. 2021; Iess et al. 2021). The KaT enables a very stable two-way coherent link in Ka band, having an Allan deviation (σ_y) of its intrinsic fractional frequency stability better than 10^{-15} at 1000 s integration time (Ciarcia et al. 2013, 2019; performances at levels of $\sigma_y \sim (4$–$5) \times 10^{-16}$ at 1000 s integration time have been measured on ground). The unit also implements a ranging channel based on PN codes at 24.35 Mcps, enabling a centimeter-level precision (two-way). The range jitter σ_ρ is proportional to S/N$^{-1/2}$; it is worth mentioning that recent measurements from the MORE's KaT reached $\sigma_\rho < 1$ cm every 4 s at 0.3 au distance from Earth (Cappuccio et al. 2020b).

Typically, such instruments exhibit a white phase noise behavior ($S(y) \propto f^2$) in the frequency region of interest for 3GM ($\sigma_y \propto \tau^{-1}$), corresponding to 2.5 μm s^{-1} measurement accuracy at 60 s integration time. However, in very precise Doppler tracking experiments, the measurement accuracy is limited by other noise sources, mainly propagation noise (due to interplanetary plasma and Earth uncalibrated troposphere) and mechanical disturbances generated both on ground and on board the spacecraft. Dispersive noise due to solar plasma can be entirely calibrated by using the JUICE multifrequency tracking system, enabled by the two additional simultaneous X/X and X/Ka links provided by the onboard Deep Space Transponder, similarly to what was done and proven by Cassini (Bertotti et al. 2003; Tortora et al. 2012). Earth's troposphere can be calibrated by means of advanced water vapor radiometers installed close to the large ground antenna dish, while the noise contribution due to ground station electronics is typically much lower or even negligible in the end-to-end measurement accuracy. For example, the contribution from the electronics (both receiving and transmitting chains) of ESA deep-space antenna DSA-3 located in Malargüe, Argentina, has been measured to $\sigma_y \sim 1 \times 10^{-16}$ level at 1000 s s integration time (de Vicente et al. 2019), which is roughly two orders of magnitude below the end-to-end measurement accuracy ($\sigma_y(\tau = 1000$ s$) \sim 1 \cdot 10^{-14}$) expected for 3GM.

During flybys, JUICE attitude constraints set by other instruments (involving rotations due to pointing of remote sensing instruments) impose the use of a steerable 60 cm Medium Gain Antenna. Rotations of the spacecraft will therefore excite the propellant in the two spacecraft tanks, inducing a potential disruptive noisy effect on 3GM observables (Cappuccio et al. 2018, 2020c). To precisely measure the accelerations of the spacecraft structure, JUICE will host on board an HAA, another nearly recurrent unit from the Italian Spring Accelerometer (ISA) on board BepiColombo (Iafolla et al. 2007; Santoli et al. 2020). The HAA measurements can be modeled as

$$a_{\mathrm{HAA}} = \lambda(a_{\mathrm{NGA}} + a_{\mathrm{IN}}) + b_0 + n_0, \qquad (4)$$

where a_{NGA} are actual nongravitational accelerations and a_{IN} represents inertial terms (e.g., rotations and gravity gradients) due to the relative distance between the HAA sensing elements and the spacecraft center of mass, while a_{HAA} are the actual HAA acceleration readings. These quantities may differ owing to a measurement scale factor λ, a bias error b_0, and the unit intrinsic noise level n_0. ISA is designed to have an intrinsic noise at the level of 10^{-9} m s$^{-2}\sqrt{\mathrm{Hz}}$ in the 3×10^{-5} Hz to 10^{-1} Hz frequency range (Iafolla et al. 2007), and JUICE's HAA is expected to perform similarly. The accelerometer manufacturer guarantees an accuracy of the on-ground calibration at 1%, while the bias is expected to be smaller than $\sim 10^{-8}$ m s^{-2}. By this, the noise from the propellant sloshing can be assumed to be safely calibrated by the HAA down to a level compatible with the expected 3GM measurement accuracy. The knowledge of the scale factor and the bias cannot rely on ground measurements and requires in-flight calibrations. These two quantities are therefore estimated in the orbit determination procedure. Since the HAA has three different sensing elements in three orthogonal directions, this translates into adding a total of six parameters, $\lambda = (\lambda_x, \lambda_y, \lambda_z)$ and $b_0 = (b_{0x}, b_{oy}, b_{0z})$, in the vector of estimated parameters. A crucial point is that any time the HAA undergoes a power cycle, these quantities may vary owing to internal thermo hysteresis of the unit and require a new calibration, affecting the way these quantities shall be treated (either global or local parameters) in the orbit determination solution.

4. Numerical Simulations

4.1. Tour Characteristics

The Jupiter baseline tour (mission kernel 150l0a) includes 2 flybys of Europa and 21 of Callisto, while the backup tour (option 230la) also includes 2 Europa flybys but only 17 of Callisto. Table 1 reports the flyby sequence together with dates, altitude of closest approach, and mean anomaly of the corresponding moon orbit around Jupiter. The characteristics of Europa encounters are very similar for both tours: two closest approaches at an altitude of 400 km with a longitude of about 180° and a latitude of about 50° and −50°, respectively. That is, the results of the Europa gravity experiment are expected to be basically unaffected by the launch date. On the opposite, ground tracks of Callisto flybys are quite different (see Figure 6), with a rather uniform coverage of the moon with the nominal tour (panel (a)) and a prevalent coverage of the northern hemisphere with the backup option (panel (b)). Figure 1 shows the mean anomaly distribution of Callisto around Jupiter during close encounters for both tours. In the nominal tour, 14 flybys occur almost at the same mean anomaly ($\sim$255°). Two other flybys occur at 28°, and another five nonredundant ones at 289°, 67°, 356°, 194°, and 265°, out of the last seven have an altitude higher than 3000 km and therefore a fainter gravity signal.

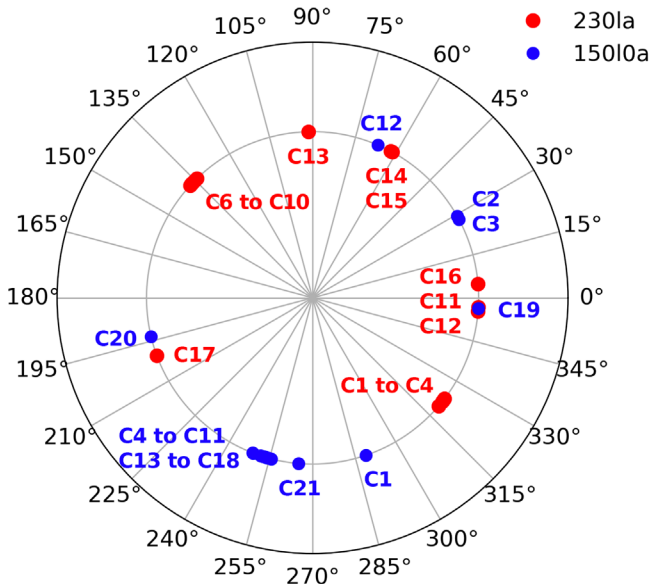**Figure 1.** Callisto flybys' mean anomaly distribution. The flybys of the nominal tour 150l0a are shown in blue, and those for the backup launch option are in red.

The flybys of the backup tour are grouped around 322°, 0°, 62°, and 136° mean anomalies, while two other nonredundant ones are at 200° and 90°. All closest approaches are at an altitude below 3000 km. The backup option represents therefore a more robust experimental scenario for measuring Callisto tides, but it provides a worse global reconstruction of the moon's gravity field with respect to the nominal tour.

4.2. Dynamical Model and Filter Setup

The simulation setup of the Europa and Callisto gravity experiments is very similar. The dynamical model includes point-mass gravity from the Sun, planets, and major Jupiter moons. For Jupiter's zonal field we have used the results from Durante et al. (2020). The nominal values of both the Europa and Callisto quadrupole coefficients have been taken from measurements carried out by the Galileo mission (Anderson et al. 1998, 2001). Higher gravity coefficients for Callisto have been synthetized following Kaula's rule (see Equations (6) and (7), from Equations (5.15) and (5.13) given by Kaula 2000) with an A_k equal to 1, assuming a similar strength of Titan gravity field (Iess et al. 2012; Durante et al. 2019). This empirical rule is representative of the gravity field of rocky bodies, while its application to icy satellites has not been demonstrated yet. It is likely that it is applicable to the rocky interior of the moons, while the outer ice layer may give rise to a quite different gravity signal. In any case, since we report on a covariance analysis, the nominal values of model parameters do not affect the results for the uncertainties. The gravity field has therefore been approximated as

$$\overline{C}_l \sim A_k \frac{10^{-5}}{l^2} \tag{5}$$

$$\overline{C}_l = \sqrt{\frac{1}{2l+1}\sum_m \overline{C}_{lm}^2 + \overline{S}_{lm}^2}. \tag{6}$$

The JUICE spacecraft has almost $\sim$90 m^2 solar arrays, and accelerations induced by the solar radiation pressure (SRP) are at level of $\sim$10^{-11} km s^{-2}. Over just a single tracking pass duration ($\sim$8 hr) the integrated acceleration can produce a net effect of $\delta v \approx 300$ mm s^{-1}, and uncertainties on the knowledge of surfaces' thermo-optical properties may affect the final covariance solution if not properly accounted for. Other nongravitational perturbations may be even larger (e.g., wheel off-loading and thrusters' firings), but they will occur outside of the 3GM measurements' windows. By limiting the data analysis to tracking passes around the flyby, the multiarc approach allows keeping the dynamical model rather simple, basically limited to gravity and SRP.

Tables 2 and 3 summarize all the estimated parameters included in our orbit determination solution for both the Europa and Callisto experiment simulations, along with their a priori values and uncertainties. The spacecraft state vector is estimated 15 hr before closest approaches with the moons. For Europa and Callisto, we have not imposed the hydrostatic equilibrium constraint, i.e., $J_2/C_{22} = 10/3$. For Callisto, we have estimated the gravity field up to degree and order 9 and the tidal Love number k_2. The HAA calibration parameters λ and b_0 are treated as global parameters, even if other operational scenarios, where they are grouped, have been investigated (see the next section for further details). Both diffuse and specular thermo-optical coefficients are included in the list of estimated parameters and treated as global ones. Since range measurements are potentially affected by bias errors, we have considered one independent range bias parameter per tracking pass per station (di Ruscio et al. 2020). This is a conservative hypothesis since it has been demonstrated that the novel PN range at 24 Mcps is less affected by this undesired phenomenon. Finally, since gravity fields of celestial bodies yield information on their rotational state, we have also estimated the spin rate and the R.A. and decl. of the Callisto pole in the body-fixed reference frame, while imposing synchronous rotation. The moon's dynamical model considers the gravitational attraction of the main bodies in the solar system. However, here we used the ephemerides from Lainey et al. (2004) and computed only the partial derivatives to estimate the moon's orbital accuracies and their impact on the estimation process.

4.3. Synthetic Observables

Range and Doppler (range-rate) data are the primary observables for the 3GM gravity experiments. Since the JUICE multifrequency radio system allows for radiometric data virtually unaffected by solar plasma, we have used a constant range-rate accuracy of 3 μm s^{-1} at 1000 s for all solar elongation angles (or Sun–Earth–Probe angle), corresponding to $\sigma_y \sim 10^{-14}$, retaining roughly a 15% margin on the expected achievable accuracy. Assuming an additive white Gaussian noise (decreasing as $\sigma_y \propto \tau^{-\frac{1}{2}}$ with the integration time), we set the simulated noise on the observables to 12 μm s^{-1} at 60 s integration time. These numbers are in line with the results from BepiColombo and Juno (Durante et al. 2020; Cappuccio et al. 2020a; Iess et al. 2018). We have also investigated the contribution of range data to the final covariance matrix. Considering the link budget, the range jitter is expected at 4 cm with an integration time of 300 s. However, the availability of range data during flybys is not guaranteed owing to possible S/N limitation in the link budget.

Since gravity coefficients of the two moons are estimated as part of an orbit determination solution that includes the motion of the probe with respect to Jupiter and the other moons, it is in general not sufficient to acquire data only during closest

Table 1
Sequence of Callisto and Europa Flyby with the Date of Closest Approach, Altitude, and Mean Anomaly (C = Callisto; E = Europa)

150l0a				230la			
Flyby	Date	C/A Altitude (km)	Mean Anomaly (deg)	Flyby	Date	C/A Altitude (km)	Mean Anomaly (deg)
C1	2032/6/21	3559	289	C1	2033/7/28	300	321
E1	2032/7/2	400	81	C2	2033/8/13	200	322
E2	2032/7/16	400	96	C3	2033/8/30	200	323
C2	2032/7/29	4437	28	C4	2033/9/16	200	319
C3	2032/8/14	1132	29	C5	2034/1/2	554	137
C4	2032/9/10	200	256	C6	2034/3/26	853	135
C5	2032/9/27	200	253	C7	2034/4/12	318	137
C6	2032/10/14	200	255	C8	2034/4/29	300	137
C7	2032/10/30	200	253	C9	2034/5/16	300	136
C8	2032/11/16	200	255	C10	2034/6/1	300	134
C9	2032/12/3	1219	253	C11	2034/6/28	1552	355
C10	2033/2/24	2071	252	C12	2034/7/15	1786	357
C11	2033/3/13	1162	253	E1	2034/7/26	400	350
C12	2033/5/10	313	67	E2	2034/8/9	400	3
C13	2033/6/4	200	254	C13	2034/8/22	764	91
C14	2033/6/21	200	249	C14	2034/10/26	2050	61
C15	2033/7/8	200	254	C15	2034/11/12	2905	62
C16	2033/7/24	200	252	C16	2035/2/17	1566	5
C17	2033/8/10	200	249	C17	2034/5/4	2615	200
C18	2033/11/1	316	254				
C19	2034/2/15	643	356				
C20	2034/5/1	3073	193				
C21	2034/6/24	6623	265				

approach. We will rely on one pass at closest approach, where the gravity signal is stronger, and two adjacent inbound and outbound arc segments (also called "wings"), which will help in decreasing the correlation between the state vector and gravity coefficients. Due to dynamical perturbations acting on the spacecraft, wheel desaturation maneuvers due to momentum torque disturbances may prevent the possibility of having clean arcs spanning for a full 48 hr period. Some preliminary analyses have shown that, conservatively, only a shorter quiet period (~30 hr) is guaranteed. Therefore, in this simulation we have assumed three, noncontiguous tracking windows lasting 6 hr each, centered respectively at −12, 0, and +12 hr from the closest approach (see Figure 2).

An implicit assumption on the radio-tracking observables' accuracy is that 3GM measurements are always supported by a Ka-band link. At present, ESTRACK DSA-3 and NASA DSS-25 are the only deep-space stations with this functionality. NASA has planned to equip by 2028 one station at every complex with Ka-band uplink capabilities in support of the VERITAS mission (Slobin et al. 2021). It is likely that in the 2032–2034 time frame ESA will also expand its ESTRACK network with other high-accuracy ground stations. We considered a coverage from ESTRACK stations DSA-1 (New Norcia, Australia), DSA-2 (Cebreros, Spain), and DSA-3 (Malargue, Argentina). For Callisto flybys C19 and C20 (see Table 1), we are supposed to have tracking support from NASA DSN DSS-35 (in Canberra, Australia) instead of from ESTRACK DSA-1 because the former offers better sampling of closest approaches and link continuity with DSA-3 (see Section 5.2). The synthetic observables have been simulated considering a minimum spacecraft elevation angle of 15° to account for errors that might affect low-elevation calibration data for Earth's troposphere. In addition, we accounted for any occultation of the radio link caused by Jupiter and the Galilean moons.
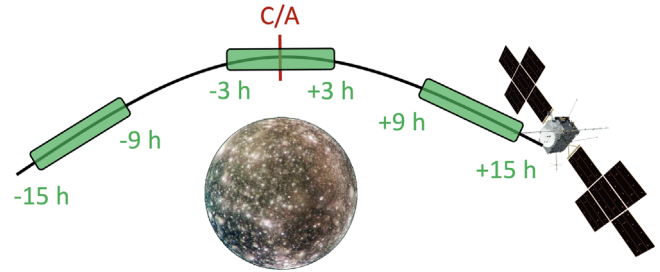

Figure 2. Representations of time slot mask for radio-tracking passes during a flyby. Note that the expected coverage from ground stations during each slot has been considered.

5. Results of Covariance Analysis

5.1. Europa

The results of the numerical simulations are reported in Table 4. Europa gravity coefficient J_2 and C_{22} can be independently estimated at the level of 3.8×10^{-6} and C_{22} at the level of 5.1×10^{-7}, an improvement by a factor 2 and 5 with respect to Galileo data, where, however, the hydrostatic constraint was adopted (Anderson et al. 1998; Gomez Casajus et al. 2021). The ratio J_2/C_{22} can be determined with an accuracy of 0.016, i.e., the hydrostatic equilibrium hypothesis can be verified at 0.5%. Thus, 3GM will be able to assess to a good level of confidence whether Europa is or is not in hydrostatic equilibrium. In Gomez Casajus et al. (2021) the data of the Galileo mission have been reanalyzed without imposing the equilibrium constraint and the ratio J_2/C_{22} is recovered with an uncertainty of 0.57, a value that is too large to allow any strong geophysical inference. If Europa will be found in hydrostatic equilibrium, the Radau–Darwin relation would allow us to estimate MoIF$_{RD}$ with an accuracy of 5.4×10^{-4}, a factor 5 better than Galileo (where the hydrostatic equilibrium constraint
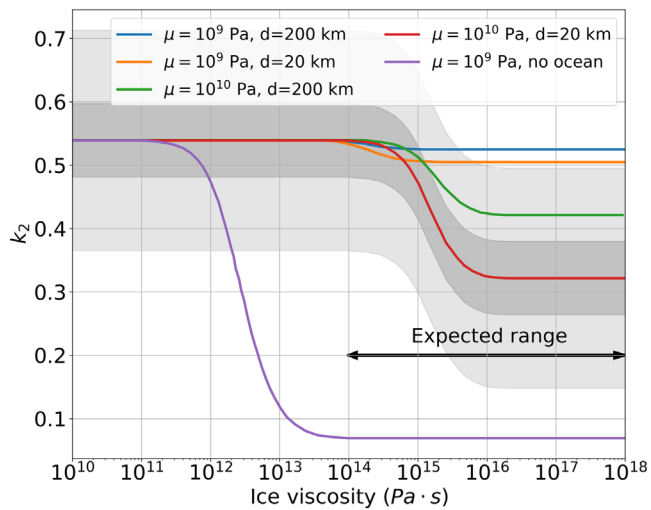
Figure 3. Callisto k_2 with and without an ocean, from Moore & Schubert (2003). The value of the Love number is reported for different values of the viscosity μ and the shell thickness d. The dark-gray shaded area represents the uncertainty, $\sigma_{k_2} = 0.059$, obtained from the numerical simulations, while the lighter-gray shaded area corresponds to $3\sigma_{k_2}$. The expected range for the ice viscosity is between 10^{14} and 10^{18} Pa s (Durham & Stern 2003 Nagel et al. 2004).

Figure 4. Callisto gravity field power of normalized coefficient. The black line represents the simulated gravity field with $A_k = 1$, the blue line is the 3σ reconstructed uncertainty with the nominal tour, and the red line is the 3σ uncertainty obtained with the backup tour. Note that for the backup trajectory the estimation of the gravity field could be limited to a lower degree.

was imposed; Anderson et al. 1998; Gomez Casajus et al. 2021). These results of the gravity experiment are obtained considering only one set of HAA calibration parameters, given the limited temporal separation between the two flybys. In the case in which the HAA is switched OFF and ON between the two flybys, the uncertainties on the estimated parameters increase by about a factor of 2.

The rotational state of Europa, and in particular its obliquity, cannot be measured by 3GM owing to the limited data set.

Lastly, the Europa ephemerides can be recovered with an accuracy of a few tens of meters along the radial and transverse direction with respect to the Jupiter system's barycenter and hundreds of meters in the out-of-plane direction, in the time frame of the Europa flybys. The velocity can be estimated with an accuracy of a few tenths of millimeters per second along the radial and transverse direction and a few centimeters per second in the out-of-plane direction. The limited time duration of the Europa gravity experiment (2 weeks from E1 to E2) causes a fast degradation of the covariance solution outside the experiment window. The determination of the moon orbit could be largely improved by combining the data of Europa Clipper (Howell & Pappalardo 2020), Galileo, and Juno, to get a single set of reconstructed ephemerides of the Galilean moons (Magnanini 2021).

5.2. Callisto

The final performances of the Callisto gravity experiment may vary according to the actual spacecraft tour and a few operational constraints of the mission that have not yet been defined. We have therefore investigated different scenarios, considering both the nominal tour (150l0a) and the backup trajectory (230la).

A key objective of the Callisto gravity experiment is the measurement of the tidal Love number k_2. This parameter not only allows us to assess the presence of an ocean but also helps in building models of the interior structure, especially by providing hints to the amount of salt dissolved in the ocean (as in the case of
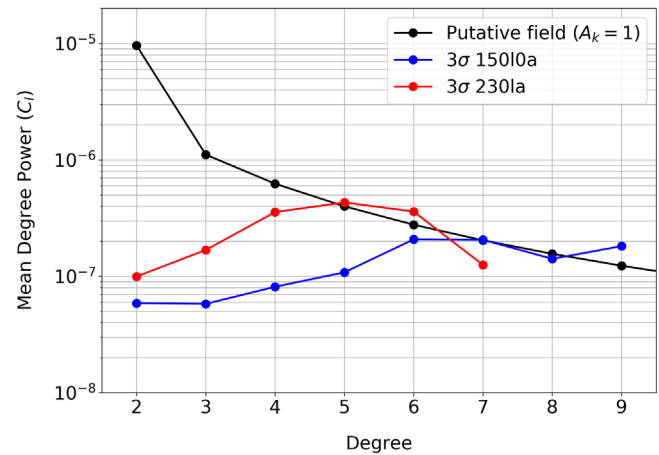
Titan, where the large k_2 is explained by a high-density ocean; Mitri et al. 2014). We find that k_2 can be estimated with a 1σ accuracy equal to 0.059, assuming a favorable case where the HAA is always ON (least set of estimated parameters). In the attempt of balancing the HAA power consumption and the number of calibration parameters to be estimated, we have assumed the HAA power cycle to occur in specific intervals. Four batches in which the accelerometer is assumed to be ON have been identified: between C1 and C9, C10 and C11, C12 and C17, C18 and C21. This implies that the HAA is turned off for about 7.5 months, saving roughly 233 MJ of energy, with a marginal impact (<2%) on the tidal estimation accuracy.

The level and type of ground coverage around the flybys' closest approach have a much more relevant impact on the measurement outcome. Our simulations indicate that with the current closest approaches' timing within the ESA baseline notional mission kernel, the switch in tracking schedule to DSA-1 (ESTRACK, New Norcia-Australia), instead of DSS-35 (DSN, Canberra-Australia), for C19 and C20 causes an increase of $\sim47\%$ in the estimation accuracy of k_2. The limitation due to the link budget may result in the loss of range data and an increase in σ_{k_2} of $\sim48\%$. In this case, one possibility could be using open-loop ranging receivers, such as the Advanced Ranging Instrument developed at NASA's Jet Propulsion Laboratory (Border et al. 2020), which will be able to recover the range measurements also in low-S/N conditions, through a software correlation.

Figure 3 shows the expected value of k_2 for different assumptions on ice viscosity, rigidity, and shell thickness, d, based on the results of Moore & Schubert (2003). We superimposed our estimated accuracy for the nominal case ($\sigma_{k_2} = 0.059$). Nagel et al. (2004) and Durham & Stern (2003) found that the expected range for Callisto ice viscosity is in between 10^{14} and 10^{18} Pa s. Thus, we can conclude that 3GM can confidently detect the presence or absence of a subsurface ocean on Callisto under the operational setup described in Section 4.3. If tracking from Canberra cannot be scheduled, the uncertainty in k_2 would increase to 0.085, but still allowing a good discrimination between an oceanless Callisto and a Callisto with an ocean. Anyhow, numerical simulation demonstrated that the support of NASA DSN's station in Canberra is very valuable for C19 and desirable also for C20.
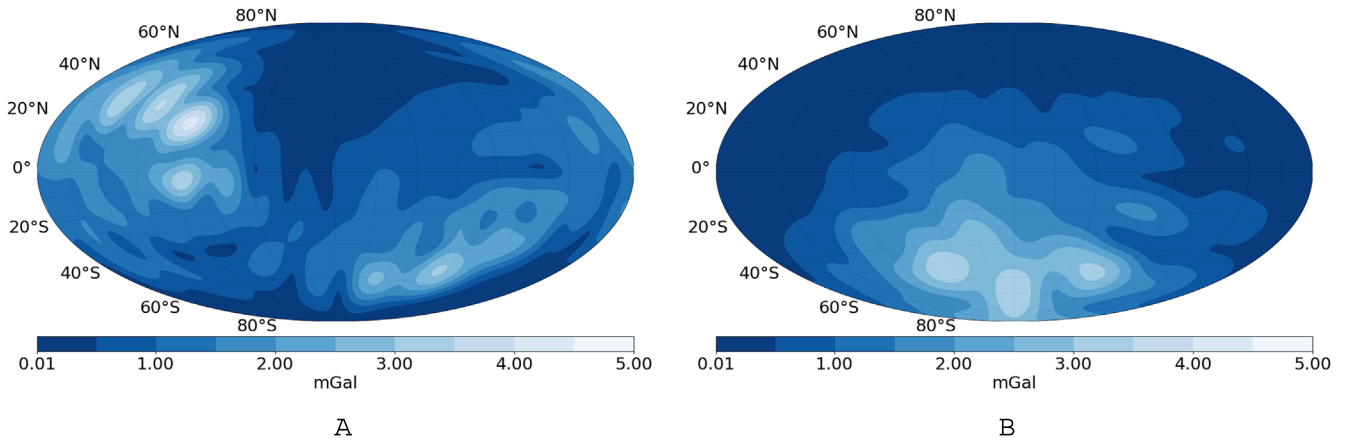
Figure 5. Callisto gravity anomaly uncertainties. Panel (a) reports the map for the nominal tour, while panel (b) reports the map of the backup tour.

Table 2
Europa Gravity Experiment Simulation Setup

Parameter	Type	Nominal Value	A Priori Uncertainty
JUICE state	Local	From kernel	Unconstrained
Europa state	Global	From ephemerides	Unconstrained
Gravity field coefficient	Global	Quadrupole coefficients from Galileo (Anderson et al. 1998)	Unconstrained
Range bias	Local	0	1.2 m
Thermo-optic coefficients	Global	Specular 0.12 Diffuse 0.12	0.5
HAA calibration parameters	Global/local	Scale factor 1.0 Bias 0	$0.01\ 1 \cdot 10^{-8}$ m s^{-2}

Table 3
Callisto Gravity Experiment Simulation Setup

Parameter	Type	Nominal Value	A Priori Uncertainty
JUICE state	Local	From kernel	Unconstrained
Callisto state	Global	From ephemerides	Unconstrained
Gravity field coefficient	Global	Quadrupole coefficients from Galileo (Anderson et al. 2001) higher terms from Kaula's rule with $A_k = 1$	Unconstrained
Gravity tide k_2	Global	0.5	1
Callisto rotational state	Global	R.A. = 268.72 deg decl. = 64.83 deg ω = 21.571 071 5 deg day^{-1} from Archinal et al. (2018)	0.1 rad 0.1 rad 1 μ rad s^{-1}
Range bias	Local	0	1.2 m
Thermo-optic coefficients	Global	Specular 0.12 Diffuse 0.12	0.5
HAA calibration parameters	Global/batches	Scale factor 1.0 Bias 0	$0.01\ 1 \cdot 10^{-8}$ m s^{-2}

Table 4
Europa Gravity Field Estimation from 3GM Experiment Simulation

$\sigma_{GM}\left(\frac{\text{km}^3}{s^2}\right)$	σ_{J_2}	$\sigma_{C_{21}}$	$\sigma_{S_{21}}$	$\sigma_{C_{22}}$	$\sigma_{S_{22}}$	$\sigma_{J_2/C_{22}}$
3.2×10^{-4}	3.8×10^{-6}	6.4×10^{-7}	3.0×10^{-7}	5.1×10^{-7}	3.3×10^{-8}	0.016

Note. The hydrostatic equilibrium constraint on (unnormalized) quadrupole coefficients is not imposed.

We have investigated the robustness of the solution by assuming the potential loss (or severe degradation) of one flyby datum, an event that may occur for several reasons, such as bad weather conditions at the ground station or possible malfunctions on board (e.g., the spacecraft entering in safe mode). With the baseline trajectory, the loss of one nonredundant flyby (C12, C19, and C20) may cause a degradation of σ_{k_2} to more than 0.1. If we consider the backup trajectory (230la), the Love number can be estimated to $\sigma_{k_2} \approx 0.04$, a 33% improvement compared to the nominal trajectory. Furthermore, we can still retrieve $\sigma_{k_2} < 0.05$ even when considering the complete data loss from any of the 17 flybys. Based on this comparison, we can reliably conclude that the backup tour offers a better opportunity to measure the Love number, although the gravity field is determined to a lower resolution.
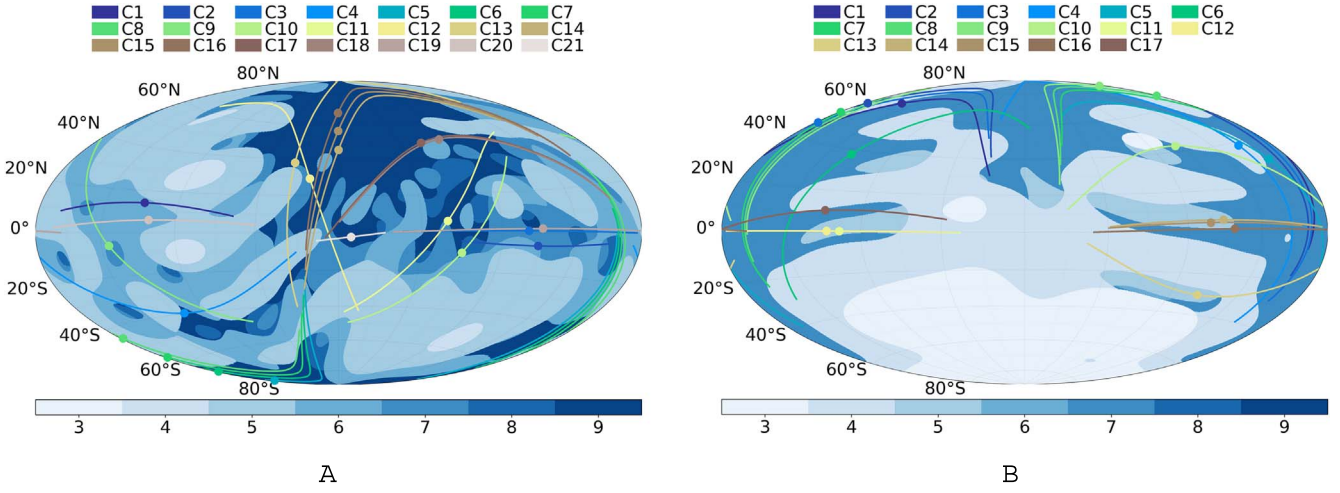
Figure 6. Callisto degree strength and JUICE ground tracks. Panel (a) reports the results for the nominal tour, while panel (b) reports the results for the backup tour.

Table 5
Callisto Gravitational Constant and Quadrupole Field Estimation from 3GM Gravity Experiment Simulation Considering the HAA Accelerometer Always ON

Tour	$\sigma_{GM}\left(\frac{km^3}{s^2}\right)$	σ_{J_2}	$\sigma_{C_{21}}$	$\sigma_{S_{21}}$	$\sigma_{C_{22}}$	$\sigma_{S_{22}}$	$\sigma_{J_2/C_{22}}$	σ_{k_2}
150l0a	9.8×10^{-5}	1.3×10^{-7}	9.9×10^{-8}	1.1×10^{-7}	1.9×10^{-8}	2.1×10^{-7}	0.014	0.059
230la	7.6×10^{-5}	1.7×10^{-7}	8.7×10^{-8}	1.3×10^{-7}	3.2×10^{-8}	8.8×10^{-8}	0.023	0.040

Note. The coefficients are unnormalized.

Table 6
Determination of Callisto Rotational State and Moment of Inertia

Tour	$\sigma_{R.A.}$ (mrad)	$\sigma_{Decl.}$ (mrad)	σ_ω (deg yr^{-1})	σ_ϵ (mrad)	$\sigma_{MoIF_{RD}}$	$\sigma_{MoIF_{\tilde{\epsilon}}}$
150l0a	14.0	2.5	0.025	5.5	4.0×10^{-4}	0.1
230la	2.6	2.0	0.012	1.6	6.8×10^{-4}	0.009

Assuming that the Callisto gravity field follows Kaula's rule with $A_k = 1$, the 3GM gravity experiment is sensitive at 3σ to the global gravity field up to degree and order 7 with the nominal tour and up to degree and order 5 with the backup option. The blue and red lines in Figure 4 report the 3σ expected uncertainty for the nominal and backup trajectory, respectively. If the real gravity field will be stronger (weaker), 3GM will be sensitive to a higher (lower) degree. Figure 5 reports the gravity anomalies' uncertainties plotted on Callisto's surface for the nominal trajectory (panel (a)) and the backup option (panel (b)). As expected, the gravity field reconstruction accuracy depends strongly on the encounters' geometry, being higher where there is better coverage (see also Figure 6).

Figure 6 reports the degree strength coverage of the Callisto gravity field (computed as per Konopliv et al. 1999), considering a 3σ uncertainty, for the nominal tour (panel (a)) and for the backup option (panel (b)). The nominal trajectory offers a good global coverage, while the backup option prefers the northern hemisphere. In the latter case, a Slepian approach (Galanti et al. 2019) to the gravity field expansion can be beneficial to reduce the numbers of solve-for-parameters and improve the resolution locally. Table 5 reports the 3GM expected results for Callisto's GM, quadrupole coefficients, and Love number k_2.

The quadrupole coefficients can be used to determine the directions of the moon's principal axes. Considering the approximation of small rotation angles, we can write the following relations (Liu & Chao 1991; Durante et al. 2019):

$$\epsilon_x = \frac{\bar{S}_{21}}{\sqrt{3}\,\bar{J}_2 - \bar{C}_{22}} \quad \epsilon_y = -\frac{\bar{C}_{21}}{\sqrt{3}\,\bar{J}_2 + \bar{C}_{22}} \quad \epsilon_z = \frac{\bar{S}_{22}}{2\bar{C}_{22}}. \tag{7}$$

The 3GM reconstructed uncertainties of the directions of the principal axes are $\sigma_{\epsilon_x} = 0°.5$, $\sigma_{\epsilon_y} = 0°.1$, $\sigma_{\epsilon_z} = 0°.6$. The latter will allow us to verify that the orientation of the principal axes of inertia is consistent with the assumed rotation model, i.e., the long axis of the inertia ellipsoid is aligned with the empty focus of Callisto's orbit, as expected for tidally locked synchronous rotators (Murray & Dermott 2000). Furthermore, the limited data set consisting of 21 Callisto flybys will not allow 3GM to significantly constrain the moon tidal phase lag.

3GM can measure the ratio J_2/C_{22} with an accuracy of 0.014, i.e., the hydrostatic equilibrium hypothesis can be verified at a level of 0.4%. If Callisto will be found in hydrostatic equilibrium, the Radau–Darwin formulation can be used to estimate the moon's polar moment of inertia with a formal accuracy of 4.0×10^{-4} (about an order of magnitude better than Galileo, where the analysis assumed hydrostatic equilibrium).

If Callisto will not be found in hydrostatic equilibrium, estimates of the MoIF are possible, with larger uncertainties, by combining gravity and topography data (see, e.g., Iess et al. 2014) or from the estimation of the moon obliquity, ϵ. Topographic data will be provided by GALA (Enya et al. 2022) and JANUS (Corte et al. 2019) instruments on board JUICE, although the final accuracy and extent of topographic products are not yet defined at this stage of the mission planning.

The spin rate, R.A., and decl. of the pole can be recovered with an uncertainty of $0°.025 \, \text{yr}^{-1}$, 14.0 mrad, and 2.5 mrad, respectively (corresponding to $0°.81$ and $0°.14$). From the latter two, the obliquity can be obtained with an accuracy, σ_ϵ, of 5.5 mrad ($0°.31$, or 13.3 km on Callisto's surface). Following the approach from Bills & Nimmo (2008), we computed the uncertainty on the MoIF under the assumption that Callisto is in a Cassini state S1 and Callisto obliquity is tidally damped. The formulation to compute the MoIF is (see Equation (19) of Bills & Nimmo 2008)

$$\text{MoIF}_\epsilon = \frac{C}{MR^2} = \frac{3}{2}\frac{n}{d\Omega/dt}\frac{[C_{22} + (C_{22}+J_2)\cos(\epsilon)]\sin(\epsilon)}{\sin(i-\epsilon)}, \quad (8)$$

where n is Callisto's mean motion, Ω is the longitude of the ascending node, i is the orbit inclination. Using this method, we obtained a reconstructed uncertainty on the moment of inertia of 0.1, which is insufficiently accurate to further constrain the interior model of Callisto. To get more accurate estimation of Callisto's MoIF without imposing hydrostaticity, an orbiter mission is more adequate (Genova et al. 2022). Table 6 summarizes these results for both JUICE tours.

Finally, the Callisto ephemerides can be recovered with an accuracy of a few tens of centimeters along the radial and transverse direction with respect to Jupiter and tens of meters in the out-of-plane direction. The velocity can be estimated with an accuracy of a few tens of microns per second along the radial and transverse direction and $\sim 100 \, \mu\text{m s}^{-1}$ in the out-of-plane direction. As for Europa, the ephemerides reconstruction can be improved by combining data sets from different missions (e.g., Europa Clipper, Galileo, and Juno; Magnanini 2021).

6. Conclusions

This work reports on the expected performance of the 3GM gravity experiment at Europa and Callisto. Through numerical simulations, we have shown that two close encounters of JUICE with Europa will allow 3GM to improve the knowledge of the quadrupole gravity field and verify the hydrostatic equilibrium hypothesis at the level of 0.5%. If this hypothesis is confirmed, the MoIF_RD can be estimated with a formal accuracy of 5.4×10^{-4}, about 0.16%. The 21 Callisto flybys, planned in the current mission scenario, will provide an estimate of the gravity field of the moon to about degree and order 7, depending on its actual strength. Furthermore, the k_2 Love number can be determined with an uncertainty of $\sigma_{k2} \sim 0.06$, sufficient to distinguish between a Callisto with or without an internal ocean, provided that the ice viscosity is in the expected range 10^{14}–10^{18} Pa · s. We verified that in a more pessimistic scenario, with a poorer ground coverage of critical flybys, 3GM would measure $\sigma_{k2} \sim 0.085$, still sufficient to distinguish between Callisto with or without an ocean. Callisto's hydrostatic equilibrium hypothesis can be tested at a 0.4% level of accuracy. If hydrostaticity will be verified, the estimate of the MoIF_RD could be quite accurate, at a level of 4.0×10^{-4}, or about 0.1% (an order of magnitude better than the Galileo estimation). If this hypothesis is disproved, 3GM

could obtain the MoIF either from the combination of gravity and shape data or through the estimation of the pole obliquity. The simulations indicate that the obliquity can be recovered with an uncertainty of 5.5 mrad, resulting in an accuracy on the Callisto moment of inertia of 0.1. This large uncertainty will not allow us to significantly constrain the interior structure of the moon. We also considered the backup trajectory, with the projected launch of JUICE in 2023 August, finding that the outcome of the Europa gravity experiment is equivalent. On the contrary, the backup orbit will let 3GM estimate the Callisto tidal Love number with an improved accuracy of $\sigma_{k2} \sim 0.04$, but with a worse global coverage of the moon's gravity.

ORCID iDs

Paolo Cappuccio ⓘ https://orcid.org/0000-0002-8758-6627
Daniele Durante ⓘ https://orcid.org/0000-0002-7888-3021

References

Anderson, J. D., Lau, E. L., Sjogren, W. L., Schubert, G., & Moore, W. B. 1997, Sci, 276, 1236
Anderson, J. D., Schubert, G., Jacobson, R. A., et al. 1998, Sci, 281, 2019
Anderson, J. D., Jacobson, R. A., McElrath, T. P., et al. 2001, Icar, 153, 157
Archinal, B. A., Acton, C. H., A'Hearn, M. F., et al. 2018, CeMDA, 130, 22
Asmar, S. W., Armstrong, J. W., Iess, L., & Tortora, P. 2005, RaSc, 40, RS2001
Bertotti, B., Iess, L., & Tortora, P. 2003, Natur, 425, 374
Bills, B. G., & Nimmo, F. 2008, Icar, 196, 293
Border, J. S., Paik, M., Lee, C., et al. 2020, Demonstration of Advanced Ranging Instrument, IPN Progress Report 42-223, Jet Propulsion Laboratory 1, https://ipnpr.jpl.nasa.gov/progress_report/42-223/42-223A.pdf
Cappuccio, P., di Benedetto, M., Cascioli, G., & Iess, L. 2018, AdAnS, 167, 3551
Cappuccio, P., di Ruscio, A., Iess, L., & Mariani, M. J. 2020a, in AIAA Scitech 2020 Forum (Reston, VA: AIAA), 1
Cappuccio, P., Hickey, A., Durante, D., et al. 2020b, P&SS, 187, 104902
Cappuccio, P., Notaro, V., di Ruscio, A., et al. 2020c, ITAES, 56, 4984
Carr, M. H., Belton, M. J. S., Chapman, C. R., et al. 1998, Natur, 391, 363
Ciarcia, S., Simone, L., Gelfusa, D., et al. 2013, in TTC 2013 VI ESA Int. Workshop on Tracking, Telemetry and Command Systems for Space Applications (Piscataway, NJ: IEEE)
Ciarcia, S., Campagna, M. G., Coletti, M., Simone, L., & Gelfusa, D. 2019, in VIII ESA Int. Workshop on Tracking, Telemetry and Command Systems for Space Applications (Noordwijk: ESA)
Corte, V. D., Noci, G., Turella, A., et al. 2019, in 2019 IEEE 5th Int. Workshop on Metrology for AeroSpace (MetroAeroSpace) (Piscataway, NJ: IEEE), 324
Darwin, G. H. 1899, MNRAS, 60, 82
de Marchi, F., di Achille, G., Mitri, G., et al. 2021, Icar, 354, 114003
de Vicente, J., Lanucara, M., Mercolino, M., et al. 2019, in VIII ESA Int. Workshop on Tracking, Telemetry and Command Systems for Space Applications (Piscataway, NJ: IEEE)
di Ruscio, A., Fienga, A., Durante, D., et al. 2020, A&A, 640, A7
di Stefano, I., Cappuccio, P., di Benedetto, M., & Iess, L. 2022, AdSpR, 70, 854
di Stefano, I., Cappuccio, P., & Iess, L. 2019, in 2019 IEEE Int. Workshop on Metrology for AeroSpace (MetroAeroSpace) 2019 (Piscataway, NJ: IEEE), 595
Durante, D., Parisi, M., Serra, D., et al. 2020, GeoRL, 47, e86572
Durante, D., Hemingway, D. J., Racioppa, P., et al. 2019, Icar, 326, 123
Durham, W. B., & Stern, L. A. 2003, AREPS, 29, 295
Enya, K., Kobayashi, M., Kimura, J., et al. 2022, AdSpR, 69, 2283
ESA SPICE Service 2020, JUICE SPICE Kernel Dataset, http://spiftp.esac.esa.int/data/SPICE/JUICE/
Fimmel, R. O., van Allen, J., & Burgess, E. 1980, Pioneer, First to Jupiter, Saturn, and Beyond (Washington DC: NASA)
Galanti, E., Kaspi, Y., Simons, F. J., et al. 2019, ApJL, 874, L24
Genova, A., Hussmann, H., Van Hoolst, T., et al. 2021, SSRv, 217, 31

Genova, A., Smith, D. E., Canup, R., et al. 2022, AcAau, 195, 68
Gomez Casajus, L., Zannoni, M., Modenini, D., et al. 2021, Icar, 358, 114187
Grasset, O., Dougherty, M. K., Coustenis, A., et al. 2013, P&SS, 78, 1
Hemingway, D. J. L., Iess, R., Tajeddine, & Tobie, G. 2018, Enceladus and the Icy Moons of Saturn, Space Science Series (Tucson, AZ: Univ. Arizona Press), 57
Howell, S. M., & Pappalardo, R. T. 2020, NatCo, 11, 1311
Hussmann, H., Spohn, T., & Wieczerkowski, K. 2002, Icar, 156, 143
Iafolla, V., Lucchesi, D. M., Nozzoli, S., & Santoli, F. 2007, CeMDA, 97, 165
Iess, L., Stevenson, D. J., Parisi, M., et al. 2014, Sci, 344, 78
Iess, L., Folkner, W. M., Durante, D., et al. 2018, Natur, 555, 220
Iess, L., Asmar, S. W., Cappuccio, P., et al. 2021, SSRv, 217, 21
Iess, L., Rappaport, N. J., Jacobson, R. A., et al. 2010, Sci, 327, 1367
Iess, L., Jacobson, R. A., Ducci, M., et al. 2012, Sci, 337, 457
Kaula, W. M. 2000, Theory of Satellite Geodesy.: Applications of Satellites to Geodesy (Mineola, NY: Dover Publications)
Kivelson, M. G., Khurana, K. K., Russell, C. T., et al. 2000, Sci, 289, 1340
Konopliv, A. S., Banerdt, W. B., & Sjogren, W. L. 1999, Icar, 139, 3
Kuskov, O. L., & Kronrod, V. A. 2005, Icar, 177, 550
Kuskov, O. L., Kronrod, V. A., & Vernadsky, V. I. 2001, Icar, 151, 204
Lainey, V., Duriez, L., & Vienne, A. 2004, A&A, 420, 1171
Lee Allison, M., & Clifford, S. M. 1987, JGR, 92, 7865
Liu, H. S., & Chao, B. F. 1991, GeoJI, 106, 699
Lupo, M. J. 1982, Icar, 52, 40
Magnanini, A. 2021, AerMS, 100, 195
McCord, T. B., Hansen, G. B., & Hibbitts, C. A. 2001, Sci, 292, 1523
McCord, T. B., Hansen, G. B., Matson, D. L., et al. 1999, JGR, 104, 11827
Milani, A., & Gronchi, G. F. 2009, Theory of Orbit Determination (Cambridge: Cambridge Univ. Press)
Mitri, G., Meriggiola, R., Hayes, A., et al. 2014, Icar, 236, 169

Moore, W. B., & Schubert, G. 2003, Icar, 166, 223
Moyer, T. 2003, Formulation for Observed and Computed Values of Deep Space Network Data Types for Navigation, JPL Publication 00-7 Jet Propulsion Laboratory, https://descanso.jpl.nasa.gov/monograph/series2/Descanso2_all.pdf
Mueller, S., & McKinnon, W. B. 1988, Icar, 76, 437
Murray, C. D., & Dermott, S. F. 2000, Solar System Dynamics (Cambridge: Cambridge Univ. Press)
Nagel, K., Breuer, D., & Spohn, T. 2004, Icar, 169, 402
Pappalardo, R. T., Belton, M. J. S., Breneman, H. H., et al. 1999, JGR, 104, 24015
Parmentier, E. M., Squyres, S. W., Head, J. W., & Allison, M. L. 1982, Natur, 295, 290
Santoli, F., Fiorenza, E., Lefevre, C., et al. 2020, SSRv, 216, 145
Schenk, P. M., McKinnon, W. B., Gwynn, D., & Moore, J. M. 2001, Natur, 410, 57
Schutz, B., Tapley, B., & Born, G. H. 2004, Statistical Orbit Determination (Amsterdam: Elsevier)
Slobin, S. D., Pham, T. T., & Chang, C. 2021, 10434-m BWG StationsTelecommunications Interfaces DSN No. 810-005, 104, Rev. NJet Propulsion Laboratory, https://deepspace.jpl.nasa.gov/dsndocs/810-005/104/104N.pdf
Spohn, Tilman, & Schubert, Gerald 2003, Icar, 161, 456
Tortora, P., Iess, L., Bordi, J. J., et al. 2012, JGCD, 27, 251
van Hoolst, T., Rose Marie, B., & Antony, T. 2013, Icar, 226, 299
Verma, A. K., & Margot, J. L. 2018, Icar, 314, 35
Vilella, K., Choblet, G., Tsao, W. E., & Deschamps, F. 2020, JGRE, 125, e06248
Zimmer, C., Khurana, K. K., & Kivelson, M. G. 2000, Icar, 147, 329